Dynamic Modeling of Battery Energy Storage and Applications in Transmission Systems

Fabian Calero, *Student Member, IEEE,* Claudio A. Cañizares, *Fellow, IEEE,* and Kankar Bhattacharya, *Fellow, IEEE*

***Abstract*—In this paper, a Battery Energy Storage System (BESS) dynamic model is presented, which considers average models of both Voltage Source Converter (VSC) and bidirectional buck-boost converter (dc-to-dc), for charging and discharging modes of operation. The dynamic BESS model comprises a simplified representation of the battery cells, which allows to simulate the effects of battery degradation, dc-to-dc converter, VSC, and the dynamics associated with the filter and transformer connecting the BESS to the grid. A decoupled dq-current control is used for the VSC, allowing the operation of the BESS in several modes, i.e., constant active and reactive power, constant power factor, voltage regulation, frequency regulation, oscillation damping, and a combination of the latter two. The proposed model is implemented in DSATools and tested for different contingencies on a benchmark system, and compared with a industry-grade BESS model used in power system dynamic studies. The importance of modeling the current control and dynamics of the dc-to-dc are demonstrated, especially when the battery cells are degraded due to, for instance, aging.**

***Index Terms*—BESS, dynamic modeling, energy storage, frequency regulation, voltage support, oscillation damping, average model.**

NOMENCLATURE

Indices

$\bar{}$	Average.
$\dot{}$	Derivative.
$\hat{}$	Per unit [pu].
o	Initial value.
d, q	d and q axis.
max, min	Maximum and minimum values.

Parameters

C_1, C_2	Dc-to-dc converter capacitors [F].
db_P, db_Q	Dead-band for frequency and voltage controllers.
dP	Rate of change limit for active power.
FL	Flags to set control modes.
K_D	Steady-state frequency droop constant.
K_{I_1}, K_{P_1}	PI control gains of current limiter control.
K_{I_2}, K_{P_2}	PI control gains of duty-cycle control.
K_{I_d}, K_{P_d}	PI control gains of current control in d axis.
K_{I_q}, K_{P_q}	PI control gains of current control in q axis.
K_{I_F}, K_{P_F}	PI control gains for frequency control.
K_{Ipl}, K_{Ppl}	PI control gains of PLL circuit.
$K_{I_{VR}}$ $K_{P_{VR}}$	PI control gains of voltage regulator.
K_{osc}	Oscillation damping gain.
K_{SoC}	SoC gain for energy integration [kWh].
K_w, T_w	Washout filter gain and time constant in P control.
L	Dc-to-dc converter inductor [H].
M_c	Number of dc converters in parallel per VSC.
N_c	Number of VSCs in parallel per BESS.
R_f, L_f	Resistance and inductance of filter and transformer [mΩ, mH].
SoC	State of charge [kWh].
T_{L_1}, T_{L_2}	Time constant for POB lead block [s].
T_{LG_1}, T_{LG_2}	Time constant for POB lag block [s].
T_{lpf}	Time constant for V_{dc} filter [s].
T_P, T_{RF}	Time constant for measurement filters [s].
T_{RV}	Time constant for measurement filters [s].
V_{bat}, R_{bat}	Equivalent battery bank voltage and resistance [V, Ω].
V_{dc_b}	DC link nominal voltage [V].
V_{nom}	Terminal ac nominal voltage [V].

Variables

d	Duty cycle of dc-to-dc converter boost switch.
I_{dc}	Current in the dclink [A].
I_L	Inductor current [A].
m_d, m_q	Modulation ratio in d and q axis.
P_s, Q_s	Active and reactive power delivered by BESS [MW, MVARr].
V_{dc}	Voltage at the terminals of the dc link [V].
V_{in}	Voltage at the battery bank terminals [V].
V_s	Terminal voltage of BESS [V].
V_t	Terminal voltage of VSC [V].
I	VSC current [A].

This work has been funded by the Natural Sciences and Engineering Research Council of Canada (NSERC) CRD grant, by the NSERC Energy Storage Technology (NEST) Network, and by a SENESCYT scholarship from the Ecuadorian government.

The authors are with the Department of Electrical and Computer Engineering, University of Waterloo, Waterloo, ON, N2L 3G1, Canada (e-mail: fcalero@uwaterloo.ca; ccanizar@uwaterloo.ca; kankar@uwaterloo.ca).

I. INTRODUCTION

AS the penetration level of renewable generation increases in transmission systems, issues such as grid stiffness, reduction in transmission flexibility, larger frequency deviations due to reduction of system inertia, and grid stability are becoming more relevant [1]. As a result, Battery Energy Storage Systems (BESSs), which have proved to be effective in facilitating the integration of renewable resources, are being

deployed worldwide, not only for small-scale applications, but also bulk transmission systems. Hence, appropriate models are necessary to better understand the potential contributions of BESS in a large-scale grid context.

Some models have been proposed for grid scale applications, such as in [2] and [3], where mathematical models of a generic Energy Storage System (ESS) are proposed, modeling the dc side of the converter and the Voltage Source Converter (VSC) as a STATCOM with a decoupled dc current control; the proposed generic controls do not allow to pursue simultaneous operational modes of the BESS. In [4], models to represent the internal characteristics of different types of batteries are described; even though the proposed models consider battery parameters like aging, State of Charge (SoC), and the effects of cycling, their effectiveness is not demonstrated in a test power system, and the models are too detailed for dynamic studies of large power networks. In [5], an average model of a BESS connected to the grid is presented, and the effects of the SoC and battery aging on the stability of the BESS is analyzed; however, in this work, the dc-to-dc converter modeled separately from the VSC, and the VSC controls are not included, nor are they tested in a power system. The application of a BESS coupled with an STATCOM to increase the transient stability of power systems is presented in [6], where the BESS provides active power and reactive power compensation is given by the STATCOM, thus providing Power Oscillation Damping (POD) services, and improving the system recovery after severe disturbances; the dynamics of the dc-to-dc converter are neglected in this model.

A BESS model is presented and tested in [7] to improve the frequency and voltage stability of a power grid, supported by a STATCOM. PI-lead and lead/lag regulators are proposed for the BESS, and their effectiveness is compared with traditional PI-based controllers in a multimachine system. Independent control branches for frequency and voltage regulation are used, which act on active and reactive power controllers that generate reference current signals used in the current controller. This work, however, does not consider the dc-to-dc converter, nor the simultaneous provision of multiple services simultaneously such as frequency regulation and oscillation damping; also, a detailed 3-phase VSC model is used instead of an average model, and there are no comparison with respect to other existing models. In [8], control strategies to improve the voltage regulation of a dc-link and dynamic performance of a BESS are presented, considering a reduced-size capacitor at the dc-link. An average dynamic model of a BESS is defined based on average techniques for both ac-to-dc and dc-to-dc converters. The duty ratio of the dc-to-dc converter is controlled through a feed-back/feed-forward control, which contributes to the reduction of the dc-link voltage variations to improve the BESS performance. However, as in [5], the VSC and dc-to-dc converters are treated separately and not integrated into a single BESS model, while controls for frequency, oscillation damping and ac voltage regulation are not considered.

Some BESS dynamic models have been proposed for microgrids, which due to their intrinsic unbalance condition require three-phase and detailed representations. For example, in [9], detailed and approximate three-phase BESS models, including average models, are proposed and compared through dynamic simulations when connected to a benchmark microgrid. Although the proposed average model considers the battery buck/boost converter, and VSC converter, it does not consider the provision of multiple services simultaneously, such as frequency regulation and oscillation damping. On the other hand, highly simplified dynamic BESS models have been proposed for frequency regulation studies, as in [10]–[13]. For example, in [13], a BESS is represented by a first-order transfer function including two control loops, one for PFR and a derivative component to provide virtual inertia in power systems with a significant number of inverter-based generators.

The Western Electricity Coordinating Council (WECC) has developed parametrizable dynamic models of BESS for transient stability studies, which are widely used in research and by industry [14]. The proposed BESS model mostly concentrates on the controls of the VSC for frequency regulation, constant PQ control, constant power factor control, and voltage regulation with droop characteristic. The control strategies of this model including an SoC control, are tested in [15], and validated with real data in [16]. In [17], an improvement of the model in [14] is proposed. However, the WECC models explicitly neglect the dc-to-dc converter, does not explicitly include oscillation damping control, neither secondary frequency regulation control, and the simplified current control used does not consider the existing coupling between current and voltages in the d- and q-axis, neither modulation index limits, which are relevant during transients.

Based on the aforementioned literature review, it can be observed that most of the previously reported BESS models neglect the dynamics of the dc side converters and controllers and battery cells in analysis for power systems, lack the capability to provide simultaneous modes of operation, and/or do not consider the BESS interacting with the grid. By including these characteristics in the BESS model, the effects of the dc-to-dc controllers' limits and dynamic response, on the ac side can be studied. Furthermore, modeling the dc-to-dc converter allows representing different types of battery banks with more realistic models. Such representation can be useful to model and study the effects of the degradation, aging, and SoC on the battery cells in existing BESS facilities, which has not yet been studied. Finally, appropriate controllers that allow the BESS to provide multiple services simultaneously, such as frequency regulation and oscillation damping, would permit to fully explore and demonstrate its potential when connected to a power grid. Hence, the main objective of this work is to propose, demonstrate, and validate with respect to existing models a generic dynamic average model of a BESS, including a simplified model for the battery bank, VSC, bi-directional buck-boost converter, ac filter, and associated controls, suitable for modeling bulk BESS facilities connected to a transmission system. Accordingly, the main contributions of this work are:

- Model the battery banks and dc-to-dc converter and its controls, integrated at the dc side of the VSC, in an average BESS model for transmission system dynamic studies. This model can be parametrized to simulate new

or existing BESS facilities, in which the degradation of the battery cells can be considered.
- Demonstrate the relevance of modelling the dc side of a bulk BESS facility connected to a transmission system, for applications such as frequency regulation, voltage control, and transient stability, showing specifically the effects of degradation of the battery cells and limits in the dc-to-dc converter controller on the dynamic response of the BESS.
- Propose and validate, by comparing with respect to existing models, an average BESS model that considers the VSC, bi-directional buck-boost converter, ac filter, and associated controls.
- Demonstrate the effectiveness of a proposed oscillation damping controller, secondary frequency regulation controller, and voltage controller, and the contributions of a large BESS to the stability of a transmission system.
- Demonstrate the adequacy of the proposed model for integration in a commercial-grade software package used for dynamic analysis of power systems, comparing its performance with existing and well-accepted models in the presence of contingencies.

The rest of the paper is organized as follows: Section II describes the main components of a BESS system, and the proposed BESS model is described in detail. In Section III, the results of simulations of the proposed BESS model providing different services in a benchmark test system is presented. Main conclusions, contributions, and possible future work are discussed in Section IV.

II. BESS Model

A BESS comprises several electrochemical cells connected in different configurations, bidirectional buck-boost converters (dc-to-dc converter), VSCs (dc-to-ac converter), filters at the Point of Common Coupling (PCC) to the grid, and the respective controls for each converter [18], as depicted in Fig. 1. Here, as illustrated in Fig. 2, a large scale BESS is modeled as N_c identical VSCs connected in parallel sharing the same amount of active and reactive power. Each individual VSC has its own filter, and is fed at its dc side by M_c equally-sized dc-to-dc bi-directional buck-boost converters connected in parallel, which share the converter's power.

The models and controls of the VSC, presented next, are developed for one of the N_c VSCs; hence, the total power of the BESS is equal to the output power of one VSC multiplied by N_c. Likewise, the active power supplied by each dc-to-dc converter is equal to the BESS power divided by the multiplication of N_c and M_c. The model proposed here is a single-phase fundamental-frequency equivalent with a dq reference frame controller that can be readily integrated in power system simulation packages for dynamic studies.

A. Battery Bank Model

The battery bank module comprises battery cells connected in series and parallel to achieve the desired voltage and power at each dc-to-dc converter. Here, a simple model comprising a voltage source V_{bat} in series with a resistor R_{bat} is considered

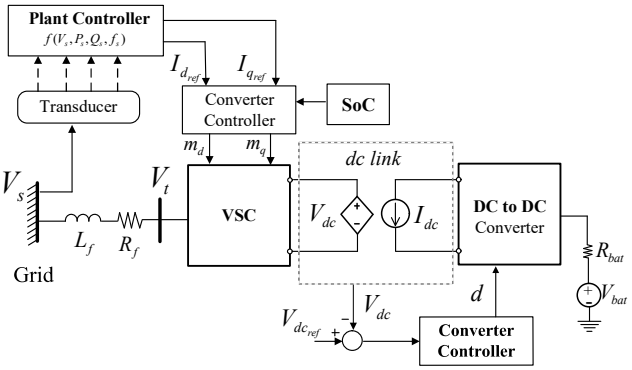


Fig. 1. Block diagram of the BESS complete model for each VSC and dc-to-dc converter.

[5], [19], as illustrated in Fig. 1. These two parameters have been used in [5] and are hence used here to approximately represent battery degradation due to aging and the impact of SoC on the battery bank, where a low battery voltage and large resistance signify a degraded battery, or a battery operating with a low SoC.

B. DC-to-DC Converter Model

An average model per switching period of a bi-directional buck-boost converter is considered here. When the dc-to-dc converter operates in boost mode (discharging mode), the magnitude of the current source I_{dc} representing the VSC load at the dc-to-dc converter's terminals is positive, and is negative when it operates in buck mode (charging). The boost and buck switches are controlled by complementary signals, i.e., $d + d_{buck} = 1$. Finally, it is assumed that the converter's inductor always operates in continuous conduction mode. Hence, the corresponding block depicted in Fig. 1 can be modeled as follows, based on [20]:

- For $0 < t \leq dT_s$ and $d_{buck}T_s < t \leq T_s$:

$$\frac{d}{dt}\begin{bmatrix} V_{in} \\ V_{dc} \\ I_L \end{bmatrix} = \begin{bmatrix} -\frac{1}{C_2 R_{bat}} & 0 & -\frac{1}{C_2} \\ 0 & 0 & 0 \\ \frac{1}{L} & 0 & 0 \end{bmatrix} \begin{bmatrix} V_{in} \\ V_{dc} \\ I_L \end{bmatrix} + \begin{bmatrix} \frac{1}{C_2 R_{bat}} & 0 \\ 0 & -\frac{1}{C_1} \\ 0 & 0 \end{bmatrix} \begin{bmatrix} V_{bat} \\ I_{dc} \end{bmatrix} \tag{1}$$

- For $dT_s < t \leq T_s$ and $0 < t \leq d_{buck}T_s$:

$$\frac{d}{dt}\begin{bmatrix} V_{in} \\ V_{dc} \\ I_L \end{bmatrix} = \begin{bmatrix} -\frac{1}{C_2 R_{bat}} & 0 & -\frac{1}{C_2} \\ 0 & 0 & \frac{1}{C_1} \\ \frac{1}{L} & -\frac{1}{L} & 0 \end{bmatrix} \begin{bmatrix} V_{in} \\ V_{dc} \\ I_L \end{bmatrix} + \begin{bmatrix} \frac{1}{C_2 R_{bat}} & 0 \\ 0 & -\frac{1}{C_1} \\ 0 & 0 \end{bmatrix} \begin{bmatrix} V_{bat} \\ I_{dc} \end{bmatrix} \tag{2}$$

where all parameters and variables in these and other equations and controls are defined in the nomenclature section. Calculating the average per switching period T_s of (1) and (2), since $\dot{\bar{x}} = d\ f_1(x) + (1-d) f_2(x)$, where $x = [V_{in}\ V_{dc}\ I_L]^T$, and

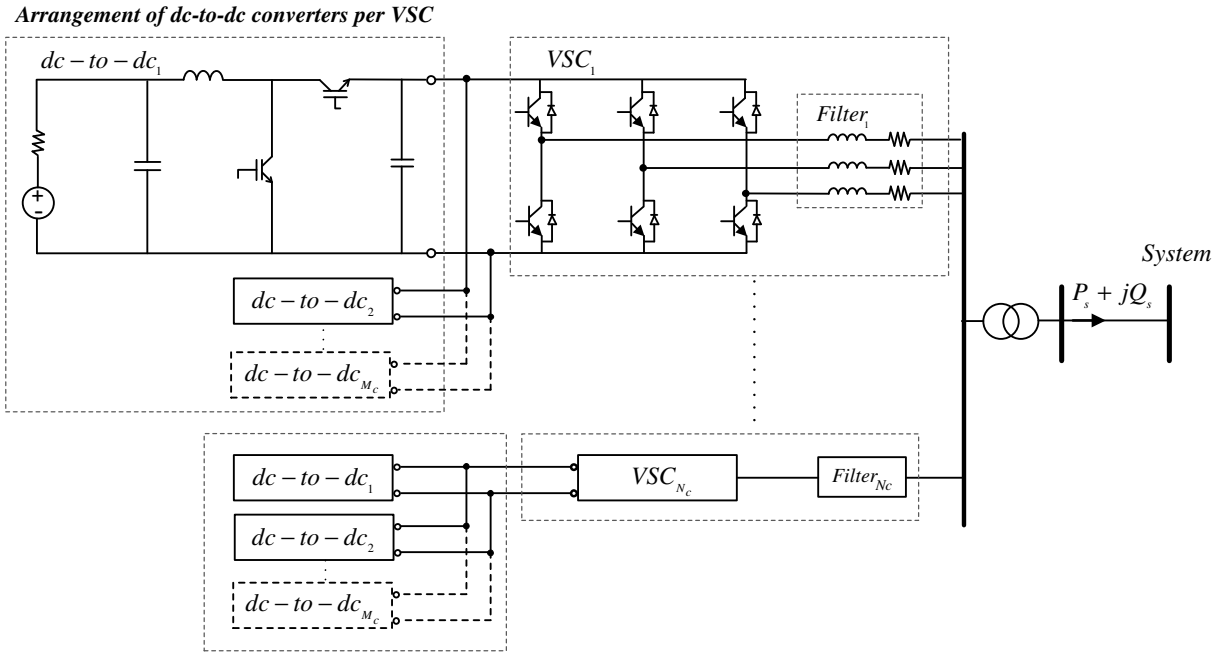


Fig. 2. BESS topology.

f_1 and f_2 are the right-hand-side of equations (1) and (2), respectively, it follows that:

$$\dot{\overline{V}}_{in} = -\frac{1}{C_2 R_{bat}}\overline{V}_{in} - \frac{1}{C_2}\bar{I}_L + \frac{1}{C_2 R_{bat}}V_{bat} \tag{3}$$

$$\dot{\overline{V}}_{dc} = \frac{1-d}{C_1}\bar{I}_L - \frac{1}{C_1}I_{dc} \tag{4}$$

$$\dot{\bar{I}}_L = \frac{1}{L}\overline{V}_{in} - \frac{1-d}{L}\overline{V}_{dc} \tag{5}$$

Assuming a lossless VSC, I_{dc} can be calculated as follows:

$$I_{dc} = \frac{P_s}{N_c M_c \overline{V}_{dc}} \tag{6}$$

C. Voltage Source Converter (VSC)

The peak phase-to-ground terminal voltage at fundamental frequency of a pulse-width modulated three-phase full bridge VSC in the dq reference frame can be calculated as [21]:

$$V_{t_d} = \frac{1}{2}m_d\overline{V}_{dc}; \quad V_{t_q} = \frac{1}{2}m_q\overline{V}_{dc} \tag{7}$$

where $\bar{V}_{dc}$ is obtained from the dc-to-dc average model. The dynamics of the filter and step-up transformer connecting the VSC to the electrical grid can be modeled by the following dq equations [21]:

$$L_f\dot{I}_d = V_{t_d} - V_{s_d} - R_f I_d + \omega_o L_f I_q \tag{8}$$

$$L_f\dot{I}_q = V_{t_q} - V_{s_q} - R_f I_q - \omega_o L_f I_d \tag{9}$$

The total active and reactive power injected by the N_c converters can be calculated as follows, considering that the decoupled dq control forces $V_{s_q} = 0$:

$$P_s = \frac{3}{2}I_d V_{s_d} N_c; \quad Q_s = -\frac{3}{2}I_q V_{s_d} N_c \tag{10}$$

D. Plant Controller

The plant controllers depicted in Figs. 3 and 4 provide the active and reactive power references to the current controller, depending on the operation of the BESS, i.e., frequency regulation, voltage support, etc. The models proposed in this section are in principle based on those presented in [14] and [17], but with the following considerable differences: the proposed models allow the BESS also provide oscillation damping, secondary frequency regulation and voltage regulation, or a combination of these. Two flags FL_P and FL_Q are used to choose the BESS operational mode, as opposed to the five flags used in [14] and [17].

1) Active Power Controls: Two main control branches are proposed in the active power controller depicted in Fig. 3: one for frequency regulation and another for oscillation damping. $\widehat{P}_{ref}$ is the power reference in per unit of the BESS nominal power S_b, which is passed to the current controller, and is equal to the summation of the initial active power reference $\widehat{P}_{ref_o}$ obtained from the solution of the power flow, plus the incremental powers $\pm\Delta\widehat{P}$ coming from the frequency regulation and oscillation damping control branches. A rate-of-change limiter is used in the frequency-regulation control path to limit the operation of the BESS when providing frequency regulation.

The control logic for the active power, presented in Fig. 3, is commanded by FL_P as follows: $FL_P = 0$ for constant P, $FL_P = 1$ oscillation damping, $FL_P = 2$ frequency regulation, and $FL_P = 3$ oscillation damping plus frequency regulation. Maximum and minimum limits $\widehat{P}_{max}$ and $\widehat{P}_{min}$ are included in the plant controller path, before $\widehat{P}_{ref}$ is passed to the current controller. When $FL_P = 0$, $\widehat{P}_{ref} = \widehat{P}_{ref_o}$ and the oscillation damping and frequency regulation branches are disabled; $\widehat{P}_{ref_o}$ is set externally to operate the BESS at a

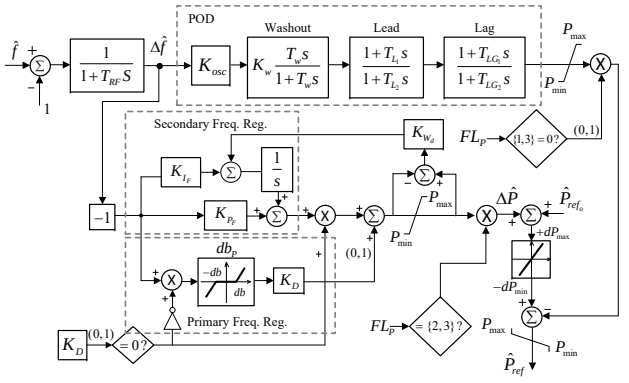


Fig. 3. Proposed control for constant P, damping oscillation, frequency regulation, and/or damping oscillation plus frequency regulation.

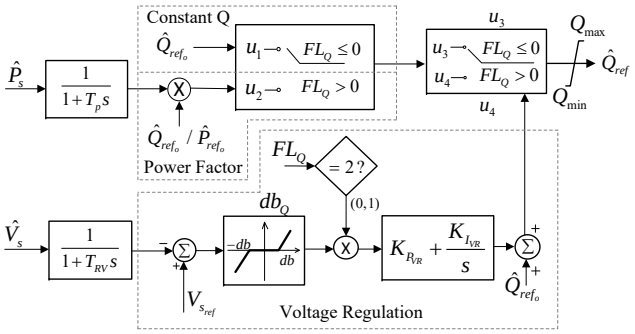


Fig. 4. Proposed control for constant Q, constant power factor, or voltage regulation.

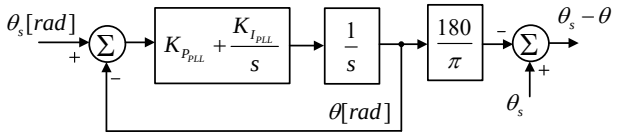


Fig. 5. Phase locked loop control.

desired active power level. A proposed oscillation damping controller is active when $FLGP = 1$, changing $\widehat{P}_{ref}$ by $\pm\Delta\widehat{P}$ as required to damp the low-frequency oscillations in the system based on the per unit frequency deviation $\Delta\hat{f}$ at the PCC, using a lead-lag block to provide the desired phase compensation (at the target frequency) between the input signal $\Delta\hat{f}$ and output power at the BESS terminals ΔP_s, while K_{osc} is used to adjust the gain of this controller. For $FL_P = 2$, the frequency regulation branch is active, while the oscillation damping branch is inactive. Unlike the models in [14] and [17], besides a constant frequency droop control, the model proposed here allows secondary frequency regulation by passing the measured $\Delta\hat{f}$ through a PI controller which brings the frequency back to its nominal value $\hat{f}_o = 1$ integrating $\Delta\hat{f}$; this control is active when $K_D = 1/R = 0$, and has anti-windup control to improve the frequency response of the BESS when it reaches limits. If $K_D \neq 0$, the secondary frequency regulation branch is automatically deactivated, and the output of the frequency regulation branch is added to $\widehat{P}_{ref}$. Finally, for $FL_P = 3$, the oscillating damping branch and the frequency regulation branch are activated at the same time, allowing the simultaneous operation of the BESS in both modes.

2) Reactive Power Controls: Three operational modes are available for reactive power control, which are independent from the operational modes of the active power control, i.e., $FL_Q = 0$ for constant Q, $FL_Q = 1$ for constant power factor, and $FL_Q = 2$ for voltage regulation. Maximum and minimum limits $\widehat{Q}_{max}$ and $\widehat{Q}_{min}$ are included in the controller path, before $\widehat{Q}_{ref}$ is passed to the current controller. In constant Q mode, $\widehat{Q}_{ref} = \widehat{Q}_{ref_o}$, where $\widehat{Q}_{ref_o}$ is the reactive power calculated at the initialization of the BESS model, which can be varied to operate the BESS at a desired reactive power. In constant power factor mode, $\widehat{Q}_{ref}$ is calculated as the multiplication of the initial ratio $\widehat{Q}_{ref_o}/\widehat{P}_{ref_o}$ times the measured $\widehat{P}_s$; this ensures that the initial power factor is maintained by changing $\widehat{Q}_{ref}$ as $\widehat{P}_s$ changes. Finally, voltage regulation is provided by comparing a measured terminal voltage $\widehat{V}_s$ to a reference value $V_{s_{ref}}$ and the difference passed through a PI controller to control the voltage at the PCC bus.

E. Current Controller

The VSC is controlled using a decoupled dq current control which is presented in Fig. 6. A PLL circuit, presented in Fig. 5 provides a reference angle θ such that the q component of the voltage at the point of connection with the electrical grid is equal to zero, i.e., $V_{s_q} = 0$; this allows the decoupling of the active and reactive power. The dq quantities are calculated as follows:

$$\widehat{V}_{s_d} = \widehat{V}_s \cos(\theta_s - \theta); \quad \widehat{V}_{s_q} = \widehat{V}_s \sin(\theta_s - \theta) \tag{11}$$

$$\hat{I}_d = \hat{I} \cos(\theta_s - \theta - \phi); \quad \hat{I}_q = \hat{I} \sin(\theta_s - \theta - \phi) \tag{12}$$

$$\phi = \tan^{-1}\left(\frac{Q_s}{P_s}\right) + \begin{cases} 0 & \text{if } P_s \geq 0 \\ \pi & \text{if } P_s < 0 \end{cases} \tag{13}$$

where θ_s and $\widehat{V}_s$ are the angle and per unit value of the voltage at the PCC bus; $\hat{I}$ is the per unit current injected by one of the N_c converters; P_s and Q_s are the active and reactive power injected by the BESS into the grid, and ϕ is the power factor angle. The bases for the per unit calculations in the dq reference frame are as follows:

$$V_b = \sqrt{\frac{2}{3}} V_{nom}, \quad I_b = \sqrt{\frac{2}{3}} \frac{S_b}{N_c V_{nom}} \tag{14}$$

The objective of the current controller is to provide the modulating signals m_d and m_q to control the converter's terminal voltage $\widehat{V}_t$ and angle θ_{V_t}, such that the BESS injected powers $\widehat{P}_s$ and $\widehat{Q}_s$ are equal to $\widehat{P}_{ref}$ and $\widehat{Q}_{ref}$, which are used to calculate $\hat{I}_{d_{ref}}$ and $\hat{I}_{q_{ref}}$. Since the decoupled control forces $V_{q_s} = 0$, the reference currents in dq components can be calculated as follows from (10):

$$\hat{I}_{d_{ref}} = \frac{\widehat{P}_{ref}}{\widehat{V}_{d_f}}, \quad \hat{I}_{q_{ref}} = -\frac{\widehat{Q}_{ref}}{\widehat{V}_{d_f}} \tag{15}$$

Where $\widehat{V}_{d_f}$ is the measurement of $\widehat{V}_d$. The currents $\hat{I}_d$ and $\hat{I}_q$ are compared with $\hat{I}_{d_{ref}}$ and $\hat{I}_{q_{ref}}$ respectively, and the error is passed through PI controllers, the output of which are the variables u_d and u_q. In order to calculate the desired VSC terminal voltages $\widehat{V}_{t_d}^{'}$ and $\widehat{V}_{t_q}^{'}$, feed forward compensation for the filter-plus-transformer inductances and grid voltages $\widehat{V}_{s_d}$ and $\widehat{V}_{s_q}$, which couple the d and q axes (see (8) and (9)), is added to the control signals u_d and u_q; these are used to calculate the VSC modulation ratio in the dq axes m_d and m_q as follows:

$$\widehat{V}_{t_d}^{'} = u_d - \widehat{X}_f \hat{I}_q + \widehat{V}_{s_d} \tag{16}$$

$$\widehat{V}_{t_q}^{'} = u_q + \widehat{X}_f \hat{I}_d + \widehat{V}_{s_q} \tag{17}$$

$$m_d = 2\left(\frac{V_b}{V_{dc_b}}\right)\frac{\widehat{V}_{t_d}^{'}}{\widehat{\widehat{V}}_{dc}^{'}}, \quad m_q = 2\left(\frac{V_b}{V_{dc_b}}\right)\frac{V_{t_q}^{'}}{\widehat{\widehat{V}}_{dc}^{'}} \tag{18}$$

where $\widehat{X}_f$ is the reactance of the filter in per unit, the variable $\widehat{\widehat{V}}_{dc}^{'}$ is the measured dc link voltage in per unit and V_{dc_b} is the nominal dc link voltage. The voltage measurement for the dc link is modeled as a low-pass filter with time constant T_{lpf}, so as to eliminate the high-frequency ripple in the dc link [22].

The control logic recommended in [14] for BESS is used here to ensure the BESS operates within its allowed SoC range. The SoC of the BESS is calculated in Fig. 6 as the integration of the active power P_s over time, where K_{SoC} is the gain conversion, and SoC_o is the initial SoC. According to the proposed logic, when the SoC becomes larger than SoC_{max} and the BESS is operating in charging mode ($\widehat{P}_{ref} < 0$), $\hat{I}_{d_{ref}}$ is forced to zero to prevent the BESS from keeping charging. On the other hand, if the SoC is less than the SoC_{min} and the BESS is operating in discharging mode ($\widehat{P}_{ref} > 0$), the $\hat{I}_{d_{ref}}$ is also forced to zero to prevent the BESS from discharging. If neither of these conditions hold, then $\hat{I}_{d_{ref}}$ passes through to the converter, operating normally. The following limits are imposed on $\hat{I}_{d_{ref}}$ and $\hat{I}_{q_{ref}}$, as proposed in [14], to prevent the BESS from exceeding its rated power:

$$\hat{I}_{d_{max}} = \begin{cases} 1 & \text{if } FL_{PQ} = 1 \\ \sqrt{1 - \hat{I}_q^2} & \text{if } FL_{PQ} = 0 \end{cases} \tag{19}$$

$$\hat{I}_{q_{max}} = \begin{cases} 1 & \text{if } FL_{PQ} = 0 \\ \sqrt{1 - \hat{I}_d^2} & \text{if } FL_{PQ} = 1 \end{cases} \tag{20}$$

When $FL_{PQ} = 1$, the BESS operates in P priority mode, and when $FL_{PQ} = 0$, it operates in Q priority mode. In the P priority mode, the current limit is smaller than the d current limit, thus providing more P and less Q outputs, and the opposite in Q priority mode.

F. DC-to-DC Controller

The dc-to-dc controller is presented in Fig. 7. Two PIs are used in cascade, the first compares the dc link voltage with a reference value, and its output (current through C_1) is added to I_{dc} to obtain a reference current thorough the inductor L, which is checked for limits and then is compared with the actual I_L. The error of the second summation is passed through a second PI, the output of which is the duty cycle of the boost switch d. This control prevents the inductor L from being overloaded, which is especially important when the batteries are degraded.

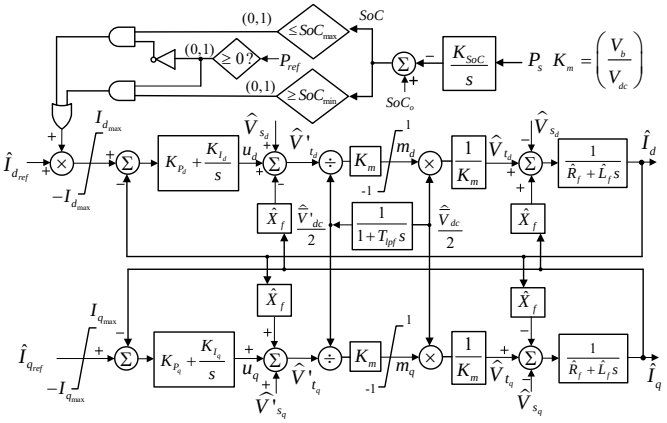


Fig. 6. Current controller in dq-Frame for VSC including the effect of the SoC in the d-axis current.

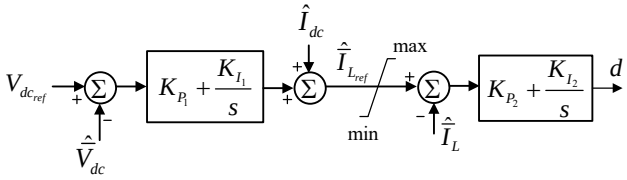


Fig. 7. DC-dc converter controller.

G. Comparison

The propose control strategy for active and reactive power is primarily based on [14] and [17], where the models discussed and validated with actual data are intended for bulk applications and practical utility studies. The concepts of plant controller, current controller, energy converter model, and their interaction discussed in [14] are adopted here as plant level controllers. However, the following controllers used within these high level blocks, which provide services associated with active and reactive power, are different with respect to those controllers discussed in [14] and [17]:

- The POD controller discussed in Section II-D-1, which includes a transducer to measure frequency and limits to prevent battery overloading.
- The control for secondary frequency regulation proposed in Section II-D-1, which includes an anti-wind-up control to improve the dynamic response of the BESS system when it has reached limits.
- The dq current controller in Section II-E.
- The dc-to-dc converter and associated controls discussed in Sections II-B and II-F, respectively.
- Besides the normal operating modes associated with active power, namely, frequency regulation, oscillation damping, and constant active power, the proposed P control logic allows simultaneous operation in frequency regulation and oscillation damping modes, as highlighted in Section II-D.

- The reactive power controller proposed in Section II-D-2 is simpler, but allows the operation the BESS in the same operating modes, i.e., voltage regulation, constant reactive power, and constant power factor mode.
- The proposed control logic requires less flags.

It should be mentioned that the average model, with some of the controls discussed in the present work have been validated with a full-detailed BESS model in an EMT-type simulations in the author's earlier work [23]. In this paper, all BESS switching phenomena are considered, comparing and validating them with the average model presented here, and demonstrating its PFR application in a detailed three-phase version of the WSCC 9-bus test system.

III. Results and Discussions

In this section, the proposed BESS model and a simplified version of it, which assumes a constant voltage at the VSC's dc link, are tested and compared with the existing BESS model proposed in [14] and with the improvements proposed in [17] in a benchmark transmission system. The effect of battery degradation, approximately modeled as both a reduction in the internal voltage of the battery cells V_{bat} and increment in the internal resistance R_{bat}, is also studied. A description of the test system, study cases for different operational modes of the BESS, and an analysis of the results of the simulations are discussed next.

A. TSAT Modeling

The simulations were performed using TSAT, which is part of the DSATools power system software package [24]. All BESS models proposed and used here were implemented as a Template User Defined Model (UDM), which allows to easily parametrize the BESS. A time step of .101ms was necessary for the simulations in TSAT to ensure convergence of the dc-to-dc converter, which represents a trade-off between accuracy of the results and simulation time. The model proposed is able to capture most of the relevant dynamics on the dc and ac side, which may bring instability to the BESS operation, which are not properly represented by models proposed in [14] and [17]. On the other hand, since average models are considered for the converters in the model proposed here, the simulation times are much faster than in detailed models, which require smaller time-steps to capture the high-frequency operation of the converter's switches.

B. Test System

The proposed BESS model was added to the WSCC 9-bus test system [25], as depicted in Fig. 8. This system is similar to the one used in [14] and [17] to validate the WECC model, with parameter values extracted from [25] - [26], and comprises three synchronous generators of which the one connected at Bus 1 is a hydro generator while the generators connected to Bus 2 and 3 are thermal units; the governors for each unit are based on [27]. IEEE type DC1A excitation systems with PSS were used for the three generators [26]. Due to the inertia constants and low damping coefficients, the test system has intrinsically low damping; hence, oscillations tent to occur when the system is disturbed. The PSSs were properly tuned to guarantee at least 5% damping coefficient in all modes of oscillation.

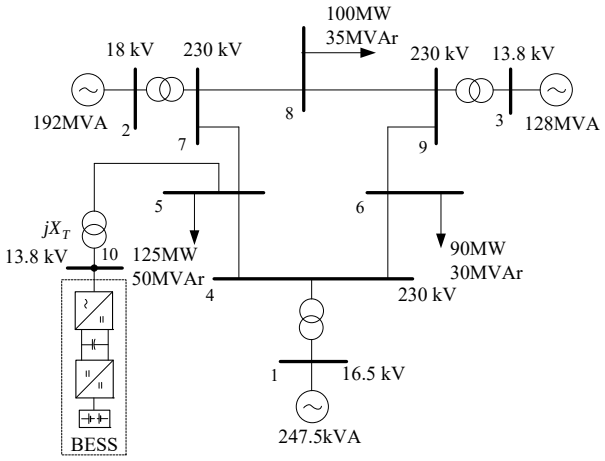


Fig. 8. BESS connected to a modified WSCC 9 bus test system.

A 45 MW BESS with the parameters given in Table I was used, which is of a similar size as the BESS used in [3] for the same WSCC system, so that the BESS can help with the frequency regulation in this system. The BESS is injecting 20 MW at Bus 10, which is latter connected to Bus 5 through a step-up transformer with a turn ratio of 13.8/230 and 0.0586 p.u. reactance. The BESS model considers an internal transformer which increases the VSC's terminal voltages from 480 V to 13.8 kV. All the BESS's PI controllers were tuned by trial and error to obtain adequate dynamic responses.

C. Study Cases

Three BESS models, as per Table II, are compared in the presented simulations for the five following different operating conditions:

TABLE I
BESS Parameters

Generator Converter					
Parameter	Value	Parameter	Value	Parameter	Value
S_b	45	V_{nom}	0.480	V_{dc_b}	900
K_D	500	K_{I_F}	2000	K_{P_F}	3000
K_W	1	T_W	0.031	T_{L_1}	0.1
T_{L_2}	0.068	T_{LG_1}	0	T_{LG_2}	0
T_P	0.02	T_{RV}	0.02	T_{RF}	0.02
db_P	0.0001	$K_{I_{VR}}$	150	$K_{P_{VR}}$	35
dP_{max}	99	K_{osc}	2552	$K_{I_{pl}}$	1400
$K_{P_{pl}}$	60	L_f	0.05449	R_f	2
T_{lpf}	0.008	K_{I_d}	0.07164	K_{P_d}	0.839098
K_{I_q}	0.07164	K_{P_q}	0.839098	N_c	30
M_c	3	R_{bat}	0.01	V_{bat}	500
L	0.0003	C_1	0.033	C_2	0.0051
K_{I_1}	296.4157	K_{P_1}	8.2048	K_{I_2}	65.5791
K_{P_2}	0.2567	db_Q	0.0001		

- Case 1: At $t = 2$s, the reactive load at Bus 5 is increased from 50 MVAr to 80 MVAr, with the BESS providing voltage regulation.

TABLE II
BESS MODELS

Name	Description	Model
Complete	Proposed complete model (Section II)	Battery + dc-dc + VSC + filter
Degraded	Sames as Complete but $R_{bat} = 0.025\Omega$ & $V_{bat} = 375V$	Battery + dc-dc + VSC + filter
Simplified	Proposed simplified model	Constant V_{dc} + VSC + filter
WECC	Model proposed in [14], [17]	VSC + filter

- Case 2: At $t = 5$s, the generator connected at Bus 3 reduces its set point by 20 MW. The proposed complete and simplified BESS models are set to provide PFR ($K_D = 500$) and SFR, while the WECC model provides PFR only, as it does not have SFR capabilities. Furthermore, the complete model is also simulated to provide the two PFR and SFR services when the battery cells are degraded.
- Case 3: At $t = 1$s, a three-phase fault occurs at Bus 8 that is cleared after 50 ms. The PSSs are disabled in all generators, and the BESS is set to provide oscillation damping only, considering as well battery cell degradation. Since the WECC model does not have this feature, it is set to operate in constant PQ mode.
- Case 4: At $t = 1$s, a three-phase fault occurs at Bus 6 that is cleared after 50 ms. The PSSs are disabled and the BESS provides oscillation damping and voltage regulation at the same time, including also battery cell degradation. Since the WECC model does not have oscillation damping capabilities, it provides voltage regulation only.
- Case 5: At $t = 1$s, the load at Bus 8 increases by 20%, the PSSs are disabled, and the BESS is set to provide PFR and oscillation damping simultaneously. Since the WECC model does not have oscillation damping capability, it is set to provide PFR only. The effects of degradation and SoC control are also studied in this case, with the SoC control parameters set as follows: $\text{SoC}_{\max}$ =2222.22 kWh or 1 p.u., $\text{SoC}_{\min}$=444.44 kWh or 0.2 p.u., and SoC_o=111.11 kWh or 0.05 p.u.

D. Results and Discussions

1) Case 1: Fig. 9 shows the voltage at Bus 5. After the fault, the BESS acts to quickly regulate the voltage, which reaches steady-state in less than a second, except when it operates in constant PQ mode; however, even with no voltage regulation from the BESS, the voltage drops up to slightly above 0.97 p.u., which is generally acceptable. Observe that all the models yield very similar responses, even when the battery cells are degraded, due to the fact that degradation limits the active power drawn from the BESS, while the reactive power is mostly dictated by control of the VSC switches and the capacitor in the dc link.

2) Case 2: The effect of battery degradation on frequency regulation is examined in this case, and the results are presented in Fig. 10 and Fig. 11. In order to simulate degradation,

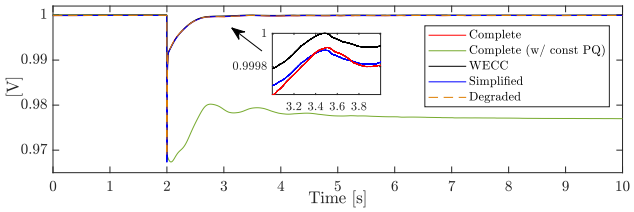


Fig. 9. Case 1 voltage at Bus 5.

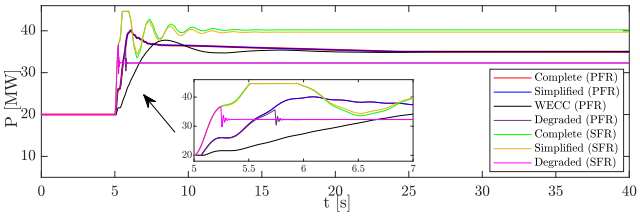


Fig. 10. Case 2 BESS active power output.

the internal battery resistance is increased to $R_{bat} = 0.025\ \Omega$ and the battery voltage is reduced to $V_{bat} = 400V$. Observe that the Complete and Simplified models are very similar for PFR, stabilizing the frequency at 59.95 Hz, with SFR bringing the frequency back to nominal in around 1 sec. Notice that when the WECC model is used, a larger frequency deviation occurs, with the frequency dropping to 59.83 Hz, thus taking longer time to stabilize (around 6 s), due to the additional PI controller in the frequency regulation path, and the absence of SFR in the WECC model. Furthermore, when degradation is simulated, the BESS output power is limited to around 32 MW, thus compromising its frequency regulation capability. The reason for this limit is that, in discharging mode, degradation implies a lower V_{in} due to a reduced V_{bat} and larger voltage drop across R_{bat}; consequently, the dc-to-dc control requires a larger inductor current I_L to realize the nominal V_{dc}, but the inductor current limiter in the dc-to-dc controller prevents I_L from increasing further, which ultimately limits the discharging current from the battery cells and the BESS output power, thus compromising the frequency regulation as shown in Fig. 11. In particular, the frequency drops to 59.86 Hz and stabilizes at 59.93 Hz, in the presence of both PFR and SFR. This behaviour can only be captured when modeling the dc-to-dc converter, which the WECC model does not consider.

3) Case 3: During the transients after the fault, all three generators and bus frequencies oscillate at a common underdamped frequency of $f = 1.335$ Hz without PSS (with PSSs active, the system is properly damped). The BESS is tuned to add damping torque to Gen 2; the lead-lag parameters are presented in Table I. Since the BESS is connected at Bus 10, $\Delta\hat{f}_{B10}$ is used as input to the POD control. After the short circuit, the oscillation damping control used in the Complete and Simplified models stabilizes the system oscillations in less than 4s, as illustrated in Fig. 12, thus proving the effectiveness of the proposed control. On the contrary, undamped oscillations are observed with the WECC model, as this does not have POD control. Similarly, when degradation is simulated

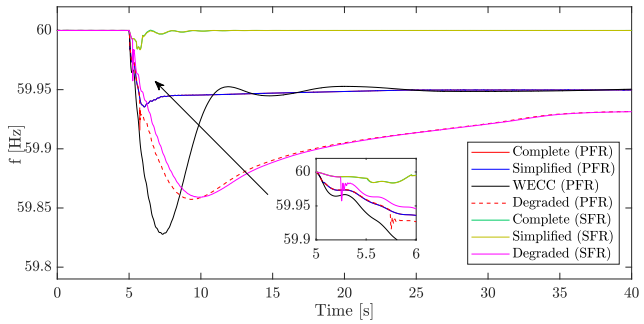


Fig. 11. Case 2 frequency at Bus 10.

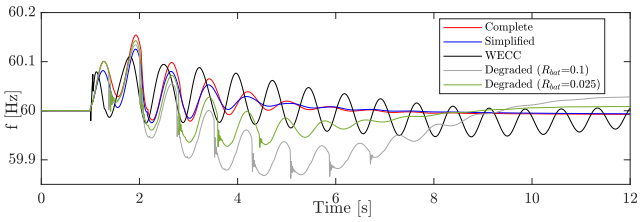


Fig. 12. Case 3 frequency at Bus 10.

(two levels in this case) the effectiveness of the control is compromised. First, the frequency further deviates after the short circuit, i.e., up to 59.93 Hz for an $R_{bat} = 0.025\ \Omega$, and 59.87 Hz for $R_{bat} = 0.1\ \Omega$. Second, the systems takes longer time to stabilize (around 11 s). Finally, damping the low frequency oscillations also takes longer (around 8 s). The reason for this is that, as in Case 2, the dc-to-dc controller limits the BESS power, which is observed as high-frequency oscillations in the degraded curves. Notice that even in the battery-degraded cases, the POD controller still manages to damp the low-frequency oscillations, albeit taking longer to do so.

4) Case 4: In Fig. 13, the simultaneous operation of the BESS for oscillation damping and voltage control is demonstrated. Observe that after the fault, the voltage at Bus 10 recovers very fast to its initial value, and the system oscillations are also damped out quickly with the Complete and Simplified models. In the Degraded case, the oscillations tend to last longer, but are also finally damped. Even though the BESS is able to regulate the voltage when the WECC model is used, undamped oscillations are observed in this case, which is due to the lack of POD control.

5) Case 5: In Figs. 14 and 15 show that the Completed, Simplified, and WECC models produced similar results. After

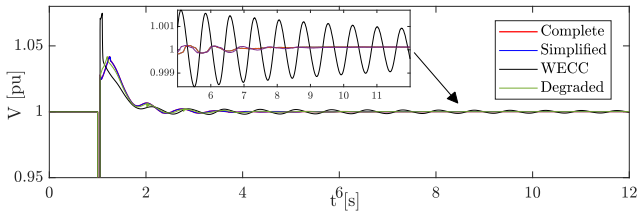


Fig. 13. Case 4 voltage at Bus 10 for BESS providing oscillation damping and voltage regulation.

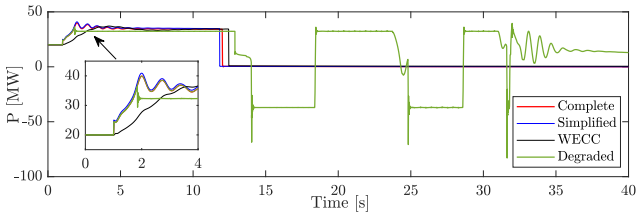


Fig. 14. Case 5 active power supplied by BESS.

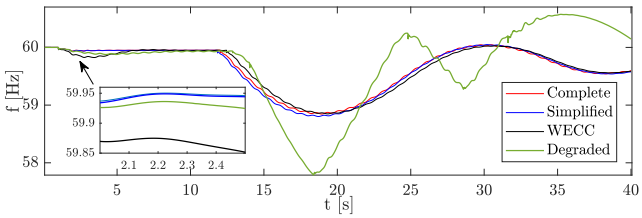


Fig. 15. Case 5 frequency at Bus No 7 with BESS providing oscillation damping and voltage regulation services.

the disturbance, the proposed PFR control stabilizes the system frequency at 59.95 Hz in less than 2 s, while the POD control simultaneously acts to damp the system low frequency oscillations. The WECC model, on the other hand, takes longer to stabilize the frequency at the same value (around 5 s), and does not damp the low-frequency oscillations. When degradation is considered, it can be observed that, again, the BESS power is limited; hence, the frequency takes longer time to stabilize (around 8 s). Once the SoC reaches its minimum value at around 12 s, the SoC control, modeled in the three cases, shuts down the BESS, leaving the frequency regulation task to the generators, which deteriorates the frequency regulation performance of the system, resulting in large low-frequency oscillations. When degradation is considered, the BESS takes longer time to reach its minimum value, due to its limited output power, resulting in frequency instability when the limit is reached, as illustrated in Figs. 14 and 15. Notice that before the SoC limits are reached, the BESS is fully capable of regulating the frequency and damp the oscillations at the same time.

IV. Conclusions

A dynamic average model of a BESS including a simplified model for the battery bank, VSC, bi-directional buck-boost converter, ac filter, and associated controls, suitable for modeling bulk BESS facilities connected to the transmission system, was proposed. This model was compared with a simplified version that neglects the dynamics of the dc-to-dc converter, and with an existing WECC BESS model for several contingencies. It was demonstrated that the additional controls proposed here for BESS, which are not considered in the WECC model, namely, SFR control and oscillation damping, can significantly improve the contribution of a large BESS to the stability of the transmission grid, and with controls with less control logic flags and regulation paths. The inclusion of the dynamics of the dc-to-dc converter and decoupled dq current control in the BESS model proved to be

relevant, especially when degradation of the battery cells were considered; however, modeling this requires a much smaller integration step depending on the software used (0.0001s in TSAT), which also increases the simulation times. Future work includes incorporating the effect of SoC on the battery internal voltage, and study the aggregated effect of distributed BESSs on the transmission grid.

REFERENCES

[1] "Contribution to bulk system control and stability by distributed energy resources connected at distribution network," IEEE PES PSDPC, Tech. Report PES-TR22, 2017.

[2] W. Du, H. Wang, L. Xiao, and R. Dunn, "Modeling energy storage systems into electric power transmission systems," in *Proc. 44th IEEE International Universities Power Engineering Conference (UPEC)*, 2009, pp. 1–5.

[3] A. Ortega and F. Milano, "Generalized model of VSC-based energy storage systems for transient stability analysis," *IEEE Trans. Power Syst.*, vol. 31, no. 5, pp. 3369–3380, 2016.

[4] A. R. Sparacino, G. F. Reed, R. J. Kerestes, B. M. Grainger, and Z. T. Smith, "Survey of battery energy storage systems and modeling techniques," in *Proc. IEEE PES General Meeting*, San Diego, USA, 2012, pp. 1–8.

[5] D. Bazargan, S. Filizadeh, and A. M. Gole, "Stability analysis of converter-connected battery energy storage systems in the grid," *IEEE Trans. Sustainable Energy*, vol. 5, no. 4, pp. 1204–1212, 2014.

[6] A. Kanchanaharuthai, V. Chankong, and K. A. Loparo, "Transient Stability and Voltage Regulation in Multimachine Power Systems Vis-Vis STATCOM and Battery Energy Storage," *IEEE Trans. Power Systems*, vol. 30, no. 5, pp. 2404–2416, 2015.

[7] U. Datta, A. Kalam, and J. Shi, "Battery energy storage system to stabilize transient voltage and frequency and enhance power export capability," *IEEE Trans. Power Syst.*, vol. 34, no. 3, pp. 1845–1857, 2019.

[8] D. Bazargan, B. Bahrani, and S. Filizadeh, "Reduced capacitance battery storage dc-link voltage regulation and dynamic improvement using a feedforward control strategy," *IEEE Trans. Energy Conversion*, vol. 33, no. 4, pp. 1659–1668, 2018.

[9] M. Farrokhabadi, S. König, C. A. Cañizares, K. Bhattacharya, and T. Leibfried, "Battery energy storage system models for microgrid stability analysis and dynamic simulation," *IEEE Trans. Power Syst.*, vol. 33, no. 2, pp. 2301–2312, 2018.

[10] D. Kottick, M. Blau, and D. Edelstein, "Battery energy storage for frequency regulation in an island power system," *IEEE Trans. Energy Conversion*, vol. 8, no. 3, pp. 455–459, 1993.

[11] H. Pia, S. Chen, H. Lv, and H. Liu, "Control strategy of battery energy storage system to participate in the second frequency regulation," in *Int. Symp. on Smart Electric Distribution Syst. and Technol. (EDST)*, Vienna, Austria, Sep. 2015, pp. 53–57.

[12] L. Liang, J. Zhong, and Z. Jiao, "Frequency regulation for a power system with wind power and battery energy storage," in *IEEE Int. Conf. on Power Syst. Technol. (POWERCON)*, Auckland, New Zealand, Nov. 2012, pp. 1–6.

[13] C. Mosca, F. Arrigo, A. Mazza, E. Bompard, E. Carpaneto, G. Chicco, and P. Cuccia, "Mitigation of frequency stability issues in low inertia power systems using synchronous compensators and battery energy storage systems," *IET Generation, Transmission, and Distribution*, vol. 13, no. 17, pp. 3951–3959, 2019.

[14] "WECC battery storage dynamic modeling guideline," Tech. report, WECC, Modeling and Validation Work Group, pp. 1–38, 2016.

[15] X. Xu, M. Bishop, D. G. Oikarinen, and C. Hao, "Application and modeling of battery energy storage in power systems," *CSEE Power and Energy Syst.*, vol. 2, no. 3, pp. 82–90, 2016.

[16] P. Pourbeik, S. E. Williams, J. Weber, J. Sanchez-Gasca, J. Senthil, S. Huang, and K. Bolton, "Modeling and dynamic behavior of battery energy storage: A simple model for large-scale time-domain stability studies," *IEEE Electrification Magazine*, vol. 3, no. 3, pp. 47–51, 2015.

[17] P. Pourbeik, "Proposal for new features for the renewable energy system generic models," Tech. report, WECC.

[18] S. Bacha, I. Munteanu, A. I. Bratcu *et al.*, *Power electronic converters modeling and control*. Springer, 2014.

[19] M. Restrepo, J. Morris, M. Kazerani, and C. A. Cañizares, "Modeling and testing of a bidirectional smart charger for distribution system ev integration," *IEEE Trans. Smart Grid*, vol. 9, no. 1, pp. 152–162, 2018.

[20] M. Kazerani, "Lecture 6: Non-isolated dc/dc converter topologies and control techniques," University of Waterloo, Spring, 2015.

[21] A. Yazdani and R. Iravani, *Voltage-sourced converters in power systems: modeling, control, and applications*. John Wiley & Sons, 2010.

[22] D. Bazargan, "A study of battery energy storage dynamics in power systems," Ph.D. dissertation, University of Manitoba, 2014.

[23] F. Calero, C. A. Cañizares, and K. Bhattacharya, "Detailed and average battery energy storage model comparison," in *IEEE PES Innovative Smart Grid Technol. Europe (ISGT-Europe)*, Bucharest, Romania, Nov. 2019, pp. 1–5.

[24] "TSAT transient security assessment tool model manual," Powertech Labs In., 2018. [Online]. Available: https://www.powertechlabs.com/

[25] P. M. Anderson and A. A. Fouad, *Power system control and stability*. John Wiley & Sons, 2008.

[26] T. Hiyama, "Rule-based stabilizer for multi-machine power system," *IEEE Trans. Power Systems*, vol. 5, no. 2, pp. 403–411, 1990.

[27] P. Kundur, N. J. Balu, and M. G. Lauby, *Power system stability and control*. McGraw-hill New York, 1994.



Fabian Calero (S'18) received the diploma in electrical engineering from Escuela Politécnica Nacional (EPN), Quito, Ecuador, in 2007. He is currently pursuing the Ph.D. degree in Electrical and Computer Engineering with the University of Waterloo, ON, Canada. His research interests include power system modeling and control, and artificial intelligence applications for dynamic modelling.



Claudio A. Cañizares (S'85,M'91,SM'00,F'07) is a University Professor and Hydro One Endowed Chair at the ECE Department of the University of Waterloo, where he has been since 1993. His highly cited research focuses on modeling, simulation, computation, stability, control, and optimization of power and energy systems. He is the IEEE Trans. Smart Gird EIC; a Fellow of the IEEE, the Royal Society of Canada, and the Canadian Academy of Engineering; and is the recipient of the 2017 IEEE PES Outstanding Power Engineering Educator Award, the 2016 IEEE Canada Electric Power Medal, and of multiple awards and recognitions from PES Technical Committees..



Kankar Bhattacharya (M'95,SM'01,F'17) received the Ph.D. degree in electrical engineering from the Indian Institute of Technology, New Delhi, India, in 1993. He was with the Faculty of Indira Gandhi Institute of Development Research, Mumbai, India, from 1993 to 1998, and with the Department of Electric Power Engineering, Chalmers University of Technology, Gothenburg, Sweden, from 1998 to 2002. In 2003, he joined the Electrical and Computer Engineering Department, University of Waterloo, Waterloo, ON, Canada, where he is currently a full Professor. His current research interests include power system economics and operational aspects. He is a Registered Professional Engineer in the province of Ontario.